Detection of the changes in dynamical structures in synchronous neural oscillations from a viewpoint of probabilistic inference

Hiroshi Yokoyama[1,2*], Keiichi Kitajo [1, 2, 3*]

1 Division of Neural Dynamics, Department of System Neuroscience, National Institute for Physiological Sciences, Okazaki 444-8585, Japan
2 Department of Physiological Sciences, School of Life Science, Graduate University for Advanced Studies (SOKENDAI), Okazaki 444-8585, Japan
3 CBS-TOYOTA Collaboration Center, RIKEN Center for Brain Science, Wako, 351-0198, Japan

* yokoyama@nips.ac.jp or kkitajo@nips.ac.jp

Abstract

Recent neuroscience studies suggest that flexible changes in functional brain networks are associated with cognitive functions. Therefore, the technique that detects changes in dynamical brain structures, which is called "dynamic functional connectivity (DFC) analysis", has become important for the clarification of the crucial roles of functional brain networks. Conventional methods analyze DFC applying static indices based on the correlation between each pair of time-series data in the different brain areas to estimate network couplings. However, correlation-based indices lead to incorrect conclusions contaminated by spurious correlations between time-series data. These spurious correlation issues of network analysis could be reduced by performing the analysis assuming data structures based on a relevant model. Therefore, we propose a novel approach that combines the following two methods: (1) model-based network estimation assuming a dynamical system for time evolution, and (2) sequential estimation of model parameters based on Bayesian inference. We, thus, assumed that the model parameters reflect dynamical structures of functional brain networks. Moreover, by introducing model parameter values prior to the Bayesian inference, the network changes can be quantified based on the comparison between prior and posterior distributions of model parameters. In this comparison, we used the Kullback-Leibler (KL) divergence as an index for such changes. To validate our method, we applied it to numerical data and electroencephalographic (EEG) data. As a result, we confirmed that the KL divergence increased only when changes in dynamical structures occurred. Our proposed method successfully estimated both network couplings and change points of dynamic structures in the numerical and EEG data. The results suggest that our proposed method is useful in revealing the neural basis of dynamic functional networks.

Author summary

We proposed a method for detecting changes in dynamical brain networks. Although the detection of temporal changes in network dynamics from neural data has become more important (aiming to elucidate the role of neural dynamics in the brain), an adequate method for detecting the time-evolving dynamics of brain networks from

neural data is yet to be established. To address this issue, we proposed a new approach to the detection of change points of dynamical network structures of the brain combining data-driven estimation of a coupled phase oscillator model and sequential Bayesian inference. As an advantage of applying Bayesian inference, which includes the model parameter values that are prior to the inference, the extent of change can be quantified based on the comparison between prior and posterior distributions. Specifically, by using the Kullback-Leibler divergence as an index for change in the dynamical structures, we could successfully detect the neuroscientifically relevant dynamics reflected as changes from prior distribution of model parameters. The results indicate that the model-based approach for the detection of change points of functional brain networks would be convenient to interpret the dynamics of the brain.

Introduction

The capacity to detect temporal changes of network dynamics from neural data has become of utmost importance for elucidating the role of neural dynamics in the brain. For instance, many neuroscience studies on the functional role of network dynamics in the brain have discussed the relevance of nonlinear coupled dynamical systems [1–4]. In addition, some recent experimental studies have suggested the possibility of flexible changes in dynamical brain networks being associated with cognitive functions and learning capacity [5–8]. However, an effective method to detect changes in dynamical structures of the brain from neural data is yet to be established.

To detect the time-varying changes in brain networks in a data-driven manner, both temporal dependence in time-series data and structural relationships within the whole brain should be considered. In general, multivariate time-series data with non-stationary dynamics, such as neuronal data, contain not only temporal dependence (i.e. causal relationship between past and current states), but also structural relationships between the variables. Most previous studies have focused on the evaluation of time-varying functional connectivity by applying the sliding window method [9, 10]. However, those prior methods are not be able to estimate the time-evolving nonlinear dynamics of a time-series data because they use correlation-based indices to estimate the connectivity strength in each time-window separately, without explicitly analyzing temporal evolution of the network dynamics [9, 10]. Furthermore, the correlation coefficient between data from two different time series tends to be larger if it contains high autocorrelation in each time-series data, regardless of the existence of a real causal relationship between data (hereafter called "spurious correlation") [11]. Therefore, the resulting networks estimated by correlation-based indices lead to an incorrect interpretation based on spurious correlations. One of the possible approaches to the abovementioned issue is using a model-based network analysis. The use of a model-based network analysis would lead to reduced spurious correlations because it would differentiate between direct and indirect couplings by assuming data structures based on a specific model. It is, however, important to select a relevant model for the estimation of network couplings because the model has to accurately explain the dynamical properties of the observed time-series data.

To address the above issues, we propose a novel model-based method to detect temporal changes in dynamical structures of functional brain networks. In this proposed method, based on the abovementioned studies on the nonlinear dynamics of the brain [1–4], we assumed that the time-evolving dynamics and the data structures of functional brain networks could be expressed as a coupled phase oscillator model. To capture the time evolution of functional brain networks, our method directly fitted the observed data to the coupled phase oscillator model [12–15] using a sequential model estimation based on Bayesian inference [16, 17]. By applying Bayesian inference, which

incorporates parameters that are prior to the inference to the model, the extent of change could be quantified based on the comparison between prior and posterior distributions. Considering such an advantage, we predicted that the temporal change in dynamical structures of the brain would be reflected in the change in model parameters. Therefore, as an index for change in dynamical structures of functional brain networks, the difference between prior and posterior distributions of model parameters was measured with the Kullback-Leibler (KL) divergence.

To validate our proposed method, the following two examinations were conducted. First, we applied our method to a time series of synthetic data with known dynamical changes of network coupling, generated by a weak coupled phase oscillator model. The purpose of this consideration was to confirm whether the change points detected by our proposed method were consistent with the true timing of network coupling changes in the synthetic data. Next, our method was applied to an open dataset of real electroencephalogram (EEG) signals measured in healthy human participants who were passively listening to binaural auditory stimuli with 40 Hz amplitude modulated white noise [18]. We then assessed whether our proposed method could detect the timing of the changes in the phase oscillatory activity induced by those periodic auditory stimuli.

Materials and methods

In this paper, we propose a new approach for the detection of change points in dynamical structures of brain networks, extending the data-driven modeling of the coupled phase oscillator model [12–15] based on sequential Bayesian inference [16, 17]. In this section, we first provide the theoretical background of the coupling oscillator model and the details of our proposed method. We then explain the procedures for model validation with synthetic data from numerical models and with electroencephalographic data.

Dynamical systems theory of phase oscillator model

In our proposed method, to estimate the dynamical structure in the functional brain networks, we applied the data-driven modeling method with the framework of phase response curve (PRC) [12, 19–22]. From the point of view of dynamical systems, the time series $X \in \mathbb{R}^{\mathrm{N}}$, which is followed by a periodic function F, could be described as $\frac{dX}{dt} = F(X)$ where N is the number of state variables. If the system exhibits limit cycles with stable point $X = X_\tau(\phi)$, the polar coordinates of this system could be written as below:

$$\frac{d\phi}{dt} = \mathrm{grad}_X\, \phi \Big|_{X=X_\tau(\phi)} \cdot F(X_\tau(\phi)) = \omega, \tag{1}$$

where ϕ, ω and τ denote phase, natural frequency, and one cycle period, respectively. Around the stable point, phase dynamics follow the periodic cycle described as $\phi(t+\tau) = \phi(t)$.

Here, we consider two coupled oscillators $X = \{x_i, x_j\}$ forced by an interaction between variables. In this case, the dynamics can be explained as:

$$\frac{dx_i}{dt} = F_i(x_i) + g_{ij}(x_j, x_i), \tag{2}$$

where $F_i(x_i)$ and $g_{ij}(x_j, x_i)$ indicate the dynamical system function of the i th oscillator and the interaction between i and j th oscillators, respectively. In the polar coordinates, the Eq (2) can expand around the stable point $X_\tau(\phi) = \{x_\tau(\phi_i), x_\tau(\phi_j)\}$ as the

following equation:

$$\begin{aligned}\frac{d\phi_i}{dt} &= \mathrm{grad}_X\, \phi\Big|_{X=X_\tau(\phi_i)} \cdot \{F(X_\tau(\phi_i)) + g_{ij}(x_\tau(\phi_i), x_\tau(\phi_j))\} \\ &= \omega + Z(\phi_i) \cdot g_{ij}(x_\tau(\phi_i), x_\tau(\phi_j))\end{aligned} \tag{3}$$

where $Z(\phi_i) = \mathrm{grad}_X\, \phi\Big|_{X=X_\tau(\phi_i)}$ indicates the function of PRC corresponding to the i th oscillator.

More generally, by averaging over one cycle, the Eq (3) could be rewritten as bellow:

$$\frac{d\phi_i}{dt} = \omega + \frac{1}{2\pi}\int_0^{2\pi} Z(\phi_i) \cdot\, g_{ij}(x_\tau(\phi_i), x_\tau(\phi_j))d\phi_i \tag{4}$$

Supposing $\phi_i = \omega t + \psi_i$ and $\omega t = \theta$, it can be rewritten as:

$$\frac{d\psi_i}{dt} \propto \frac{1}{2\pi}\int_0^{2\pi} Z(\theta + \psi_i) \cdot\, g_{ij}(x_\tau(\theta + \psi_i), x_\tau(\theta + \psi_j))d\theta. \tag{5}$$

In addition, assuming $\Theta = \theta + \psi_i$ (i.e., $\theta = \Theta - \psi_i$), the Eq (5) could be approximated as the function of phase difference $\psi_j - \psi_i$ [19,22];

$$\frac{d\psi_i}{dt} \propto \Gamma_{ij}\left(\psi_j - \psi_i\right) \tag{6}$$

$$\Gamma_{ij}\left(\psi_j - \psi_i\right) = \frac{1}{2\pi}\int_0^{2\pi} Z(\Theta) \cdot g_{ij}(x_\tau(\Theta), x_\tau(\Theta + (\psi_j - \psi_i)))d\Theta \tag{7}$$

Note that the function $\Gamma_{ij}\left(\psi_j - \psi_i\right)$ describes the interaction between i and j th oscillators.

Considering Eq (5)– (7), the Eq (4) can be extended as the function of phase difference between oscillators [19,22]:

$$\frac{d\phi_i}{dt} \approx \omega + \Gamma_{ij}\left(\phi_j - \phi_i\right). \tag{8}$$

Given the above equations, the function $\Gamma_{ij}\left(\phi_j - \phi_i\right)$ is described as phase changes in the cycle period of coupled oscillators via network interaction for each oscillator. Thus, by estimating the function $\Gamma_{ij}\left(\phi_j - \phi_i\right)$ from empirically measured data, we can characterize the coupling between oscillators. Hereafter, we call this function $\Gamma_{ij}\left(\phi_j - \phi_i\right)$ as the "phase coupling function".

Phase oscillator model approximated with the Fourier series

Some computational and methodological neuroscience studies [12–15] proposed data-driven methods to estimate the phase coupling function from observed neuronal data. In our study, the phase coupling function was approximated as P th Fourier series [12–15], and its parameters in the Fourier series were assessed by fitting the observed data to Eq (10) using Bayesian inference.

$$\frac{d\theta_i\left(t\right)}{dt} = \omega_i(t) + \Gamma_{ij}(\theta_j(t) - \theta_i(t)) + \eta_i(t) \tag{9}$$

$$\begin{aligned}\frac{d\theta_i\left(t\right)}{dt} = \hat{\omega}_i\left(t\right) + \sum_{p=1}^{P}\sum_{j\neq i}^{N}\Big\{ & a_{ij}^{(p)}(t)\cos\left[p(\theta_j(t) - \theta_i(t))\right] \\ & + b_{ij}^{(p)}(t)\sin\left[p(\theta_j(t) - \theta_i(t))\right]\Big\} + \eta_i(t)\end{aligned} \tag{10}$$

$$\text{where,} \quad \hat{\omega}_i\left(t\right) = \omega_i(t) + \sum_{j\neq i}^{N} a_{ij}^{(0)}(t)$$

Note that $\theta_i(t)$ and $\omega_i(t)$ stand for the phase and the natural frequency of the i th oscillator, respectively. Moreover, $a_{ij}^{(p)}$ and $b_{ij}^{(p)}$ indicates the coefficients of P th Fourier series corresponding to the coupling strength between i and j th oscillators. In our proposed method, the coupling strength κ_{ij} for all i, j is defined as:

$$\kappa_{ij}(t) = \sqrt{\sum_{p=1}^{P} \{a_{ij}^{(p)}(t)\}^2 + \{b_{ij}^{(p)}(t)\}^2}. \tag{11}$$

Estimation of the model parameters and change point scores

We next explain how to assess the model parameters in Eq (10) and the main idea behind change point detection from observed data. To evaluate the time-varying changes in the networks, we extended the parameter estimation algorithm in Eq (10) using Bayesian inference [16, 17]. In this way, the parameters of Eq (10) could be directly estimated from the observed data with the same manner of sequential Bayesian regression. In order to apply Bayesian inference, the Eq (10) was rewritten in its matrix form in Eq (12) .

$$\begin{aligned}
&\Theta' = \mathbf{f} \cdot \mathrm{K} + \eta \\
&\text{where,} \\
&\Theta' = \left[\frac{\theta_1(t+h) - \theta_1(t)}{h}, ..., \frac{\theta_N(t+h) - \theta_N(t)}{h} \right] \\
&\mathbf{f} = \begin{bmatrix} \mathrm{f}_1(\Theta, t) & O & \dots & O \\ O & \mathrm{f}_2(\Theta, t) & \dots & O \\ \vdots & \vdots & \ddots & \vdots \\ O & O & \dots & \mathrm{f}_N(\Theta, t) \end{bmatrix} \\
&\mathrm{f}_i(\Theta, t) = \{\cos[\theta_1(t) - \theta_i(t)], ..., \cos[\theta_N(t) - \theta_i(t)], \\
&\qquad \sin[\theta_1(t) - \theta_i(t)], ..., \sin[\theta_N(t) - \theta_i(t)], ..., \\
&\qquad \cos[p(\theta_1(t) - \theta_i(t))], ..., \cos[p(\theta_N(t) - \theta_i(t)], \\
&\qquad \sin[p(\theta_1(t) - \theta_i(t))], ..., \sin[p(\theta_N(t) - \theta_i(t)], 1\} \\
&\mathrm{K} = [\mathrm{K}_1(t), \mathrm{K}_2(t), ..., \mathrm{K}_N(t)]^T \\
&\mathrm{K}_i(t) = \{a_{i1}^{(1)}(t), ..., a_{iN}^{(1)}(t), b_{i1}^{(1)}(t), ..., b_{iN}^{(1)}(t), ..., \\
&\qquad a_{i1}^{(p)}(t), ..., a_{iN}^{(p)}(t), b_{i1}^{(p)}(t), ..., b_{iN}^{(p)}(t), \hat{\omega}_i(t)\}
\end{aligned} \tag{12}$$

Note that Θ and K stand for the vector of phase and the coefficients of the Fourier series, respectively. Moreover, Θ' indicates a time derivative of the phase with a smaller time h which is closed to 0.

Given the prior distribution of the model parameters, the parameter K in Eq (12) could be calculated by the Bayesian rule [16, 17].

$$\begin{aligned}
\Theta' &= \mathbf{f} \cdot \mathrm{K} + \eta, \qquad \eta \sim \mathcal{N}\left(0, \sigma^2 I\right) \\
\Theta' &\sim p\left(\Theta' = \frac{\Theta(t+h) - \Theta(t)}{h} \;\middle|\; \mathbf{f}, \mathrm{K}\right) \\
p\left(\mathrm{K} \mid \mathbf{f}, \Theta'\right) &\propto p\left(\Theta' = \frac{\Theta(t+h) - \Theta(t)}{h} \;\middle|\; \mathbf{f}, \mathrm{K}\right) \; p\left(\mathrm{K}\right)
\end{aligned} \tag{13}$$

Here, in our proposed method, the prior distribution $p(\mathrm{K})$ is assumed to be a multivariate normal distribution $\mathcal{N}(\mu_{\mathrm{K}}, \Sigma_{\mathrm{K}})$, where μ_{K} and Σ_{K} indicate mean and

covariance of the distribution, respectively. The update rule of the prior distribution is derived as below [16].

$$\begin{aligned} \bar{\Sigma}_{\mathrm{K}} &= \Sigma_{\mathrm{K}} - \Sigma_{\mathrm{K}}\mathbf{f}\left(\eta + \mathbf{f}\Sigma_{\mathrm{K}}\mathbf{f}^{T}\right)^{-\mathbf{1}}\mathbf{f}^{T}\Sigma_{\mathrm{K}} \\ \bar{\mu}_{\mathrm{K}} &= \mu_{\mathrm{K}} + \Sigma_{\mathrm{K}}\mathbf{f}\left(\eta + \mathbf{f}\Sigma_{\mathrm{K}}\mathbf{f}^{T}\right)^{-\mathbf{1}}\left(\Theta' - \mathbf{f}\mu_{\mathrm{K}}\right) \end{aligned} \tag{14}$$

where $\bar{\mu}_{\mathrm{K}}$ and $\bar{\Sigma}_{\mathrm{K}}$ indicate the updated mean and covariance, respectively. After the update of the prior distribution, these parameters are set as $\mu_{\mathrm{K}} = \bar{\mu}_{\mathrm{K}}$ and $\Sigma_{\mathrm{K}} = \bar{\Sigma}_{\mathrm{K}}$ for the next updating process.

Moreover, the posterior predictive distribution of the model could be inferred as the following equation.

$$\hat{\Theta}' \sim \mathcal{N}\left(\mathbf{f}\mu_{\mathrm{K}}, \mathbf{f}\Sigma_{\mathrm{K}}\mathbf{f}^{T}\right) \tag{15}$$

The update rule of Eq (15) is given below:

$$\begin{aligned} \hat{\Theta}' &= \mathbf{f}\mu_{\mathrm{K}} \\ \eta &= \mathbf{f}\Sigma_{\mathrm{K}}\mathbf{f}^{T} + \sigma^{\mathbf{2}}\mathbf{I} \end{aligned} \tag{16}$$

Note that the parameter σ^2 is a noise scaling factor of the model, and this parameter is an arbitrary constant term. Based on the above procedure, sequential change point detection based on Bayesian inference was conducted. The overview of this sequential process is shown in Fig 1.

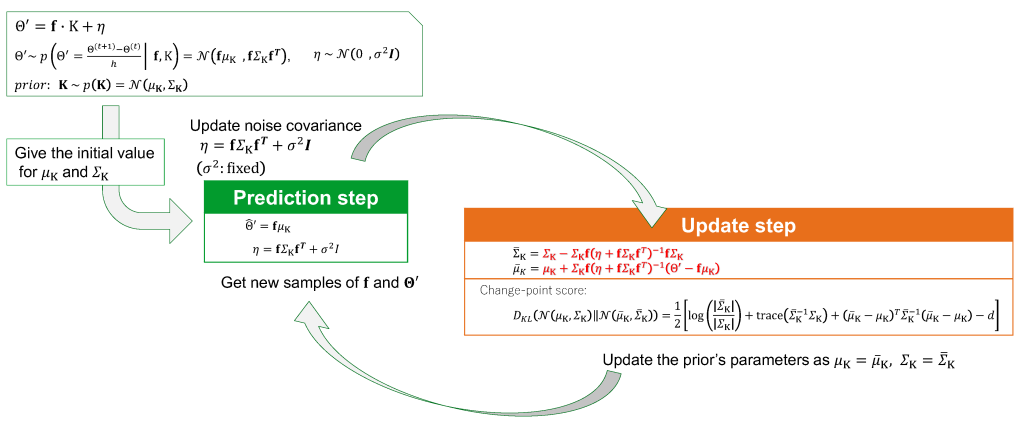

Fig 1. Schematic view of the algorithm in sequential Bayesian inference. First, after giving initial values of μ_{K} and Σ_{K} for the prior distribution, the predictive posterior distribution of the model is updated with the sequentially sampled data f and $\boldsymbol{\Theta}'$ (see "Prediction step"), and the noise covariance η is updated. Next, the prior distribution of the model parameters is updated (see "Update step"). After this, the extent of change in dynamical structures of the network is assessed with Kullback-Leibler (KL) divergence (i.e. evaluation of the change point score). The updated parameters of the prior distribution are set as $\mu_{\mathrm{K}} = \bar{\mu}_{\mathrm{K}}$ and $\Sigma_{\mathrm{K}} = \bar{\Sigma}_{\mathrm{K}}$ for the next "Prediction step".

The advantage of applying Bayesian inference to estimate the phase coupling function of dynamical networks is that the current state of the network dynamics and its dynamical structure can be expressed by a probability distribution. In other words, it means that the extent of change in the network structures can be quantified based on the comparison between prior and posterior distributions of model parameters.

Therefore, in our proposed method, the KL divergence is used as an index for the change in dynamical structures as shown in Eq (17), and the value of KL divergence is defined as the change point score.

$$
\begin{aligned}
&D_{KL}\left(\mathcal{N}\left(\mu_{\mathrm{K}}, \Sigma_{\mathrm{K}}\right) \;||\; \mathcal{N}\left(\bar{\mu}_{\mathrm{K}}, \bar{\Sigma}_{\mathrm{K}}\right)\right) \\
&\quad = \frac{1}{2}[\log\left(\frac{|\bar{\Sigma}_{\mathrm{K}}|}{|\Sigma_{\mathrm{K}}|}\right) + \mathrm{trace}\left(\bar{\Sigma}_{\mathrm{K}}^{-1}\Sigma_{\mathrm{K}}\right) + \left(\bar{\mu}_{\mathrm{K}} - \mu_{\mathrm{K}}\right)^{T}\bar{\Sigma}_{\mathrm{K}}^{-1}\left(\bar{\mu}_{\mathrm{K}} - \mu_{\mathrm{K}}\right) - d]
\end{aligned}
\tag{17}
$$

Through the above process, we can detect change points in network dynamics while sequentially estimating dynamical structures in the brain. Fig 2 shows the overview of our proposed method.

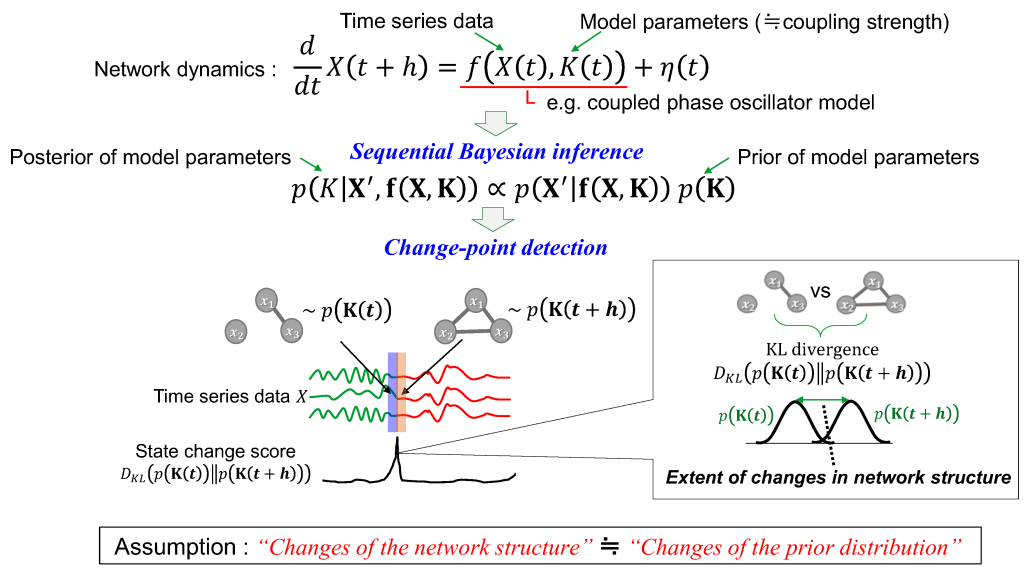

Fig 2. Overview of our proposed method for network change point detection. In our proposed method, the time series of data is fitted with a coupled phase oscillator model by Bayesian inference. We here assume that network changes are represented as the changes to the model parameters regarding coupling strength between phase oscillators. By giving the prior distribution of the model parameters, the structural changes in networks could be quantified by comparing prior and updated posterior distributions. Therefore, the changes in dynamical structures of brain networks are quantified based on the KL divergence between prior and posterior distributions.

Validation of our proposed method

Validation with numerical simulation of phase oscillator model

To validate our proposed method, we first applied our method to a time -series of synthetic data generated by Eq (10) with 1-st order Fourier series (i.e., $P = 1$).

In this validation, we considered three different simulation settings as shown in Fig 3 – 5. For all simulation settings, the number of oscillators was set to $N = 3$, and the initial value of phase angle for each oscillator was randomly selected from the range of 0 to π with $\frac{\pi}{3}$ steps. The natural frequency of each oscillator was fixed as

$$\hat{\omega} = [2\pi \cdot 3.95, \quad 2\pi \cdot 4.20, \quad 2\pi \cdot 4.62]\,.$$

For each simulation, other parameters in Eq (10) were set as shown in Fig 3B, 4B and 5B. These figures indicate actual temporal behavior of the function $\Gamma_{ij}(\theta_j(t) - \theta_i(t))$ generated by Eq (10). The temporal behavior of $\Gamma_{ij}(\theta_j(t) - \theta_i(t))$ consisted of three segments separated by two events. In the first event, the Fourier coefficients a_{ij}, b_{ij} changed, which indicated the occurrence of changes in the dynamical structure of networks in the boundary between segments 1 and 2 (hereafter, this event is called "structural change"). In the second event, the Fourier coefficients a_{ij}, b_{ij} did not change between segments 2 and 3; however, the observation noise, which does not directly contribute to temporal dynamics, drastically changed (hereafter, this event is called "noise-level change"). For each segment of all simulation conditions, the values of a_{ij} and b_{ij} were set as shown in Fig 3A, 4A, and 5A.

After generating the synthetic data by following the above procedure, our method was applied to the time series of synthetic data as below:

- Fit the time series of synthetic data to 1st order Fourier series by Bayesian inference (Fig 1)
- Evaluate KL divergence between prior and posterior of model parameters (i.e., assess the change point score; Fig 2)
- Select the time-sample that has the greater change point score relative to the threshold as the "change point"

Note that the threshold for the change point score is set as mean(KL) + 3SD(KL). The mean(KL) and 3SD(KL) stand for the mean and standard deviation, respectively, of the change point score across samples. In particular, the noise scaling factor σ^2 in Eq (16) was fixed as $\sigma^2 = 0.001$ for each simulation.

The purpose of this validation was to confirm whether our proposed method could correctly detect when changes in the dynamical structure occurred. If the assumption of our method as mentioned in the previous section is correct, the change point would be detected only in the first event, corresponding to the occurrence of changes in the dynamical structure.

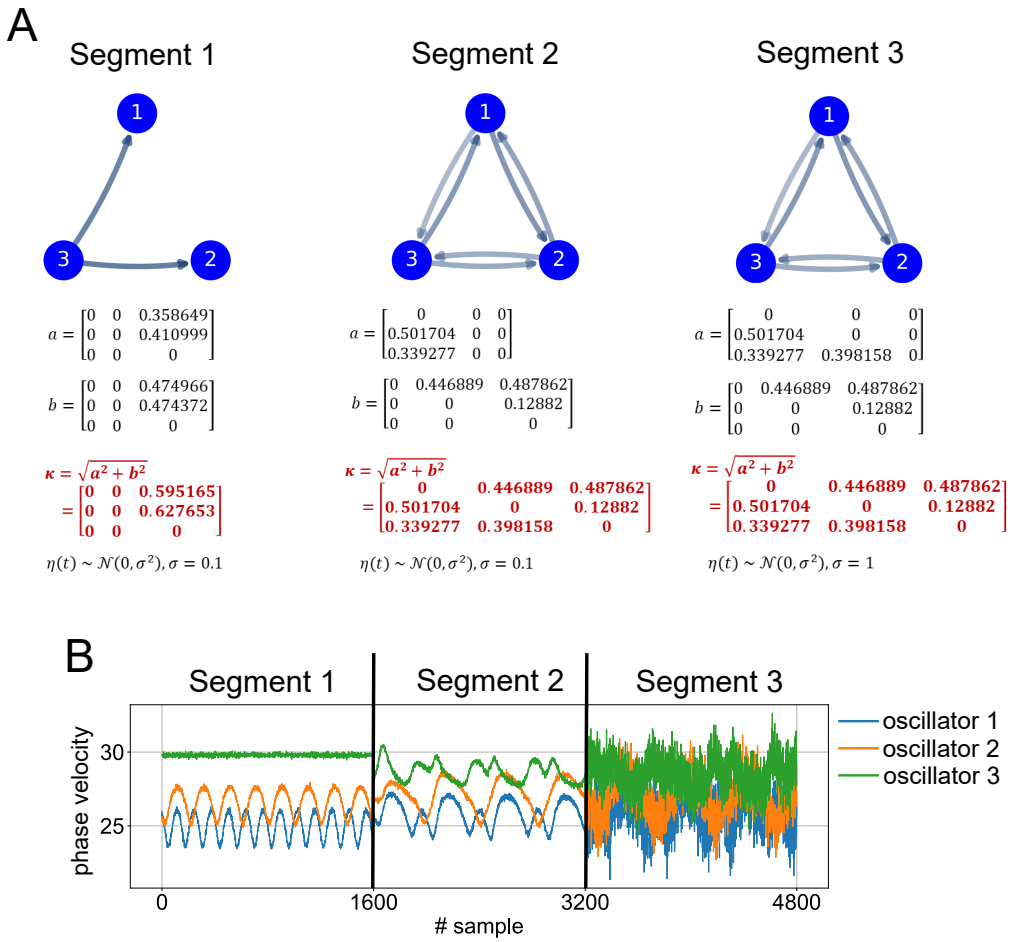

Fig 3. Parameter settings in simulation 1. (A) True network structure and parameter settings in each segment. The time series of synthetic data is generated with the function $\Gamma_{ij}(\theta_j - \theta_i)$ approximated by the 1-st order Fourier series using these parameter settings in each segment. (B) Simulated temporal behavior of the phase oscillator model.

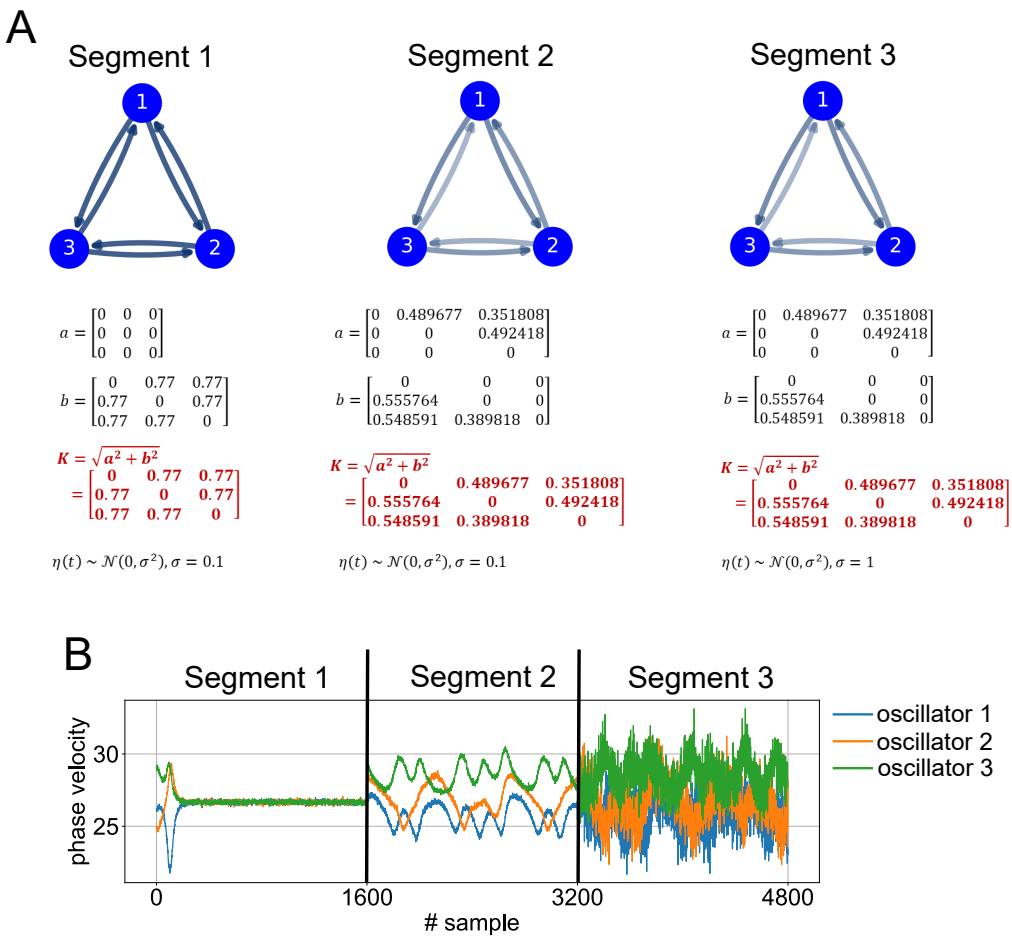

Fig 4. Parameter settings in simulation 2. (A) True network structure and parameter settings in each segment. The time series of synthetic data is generated with the function $\Gamma_{ij}(\theta_j - \theta_i)$ approximated by the 1-st order Fourier series using these parameter settings in each segment. (B) Simulated temporal behavior of the phase oscillator model.

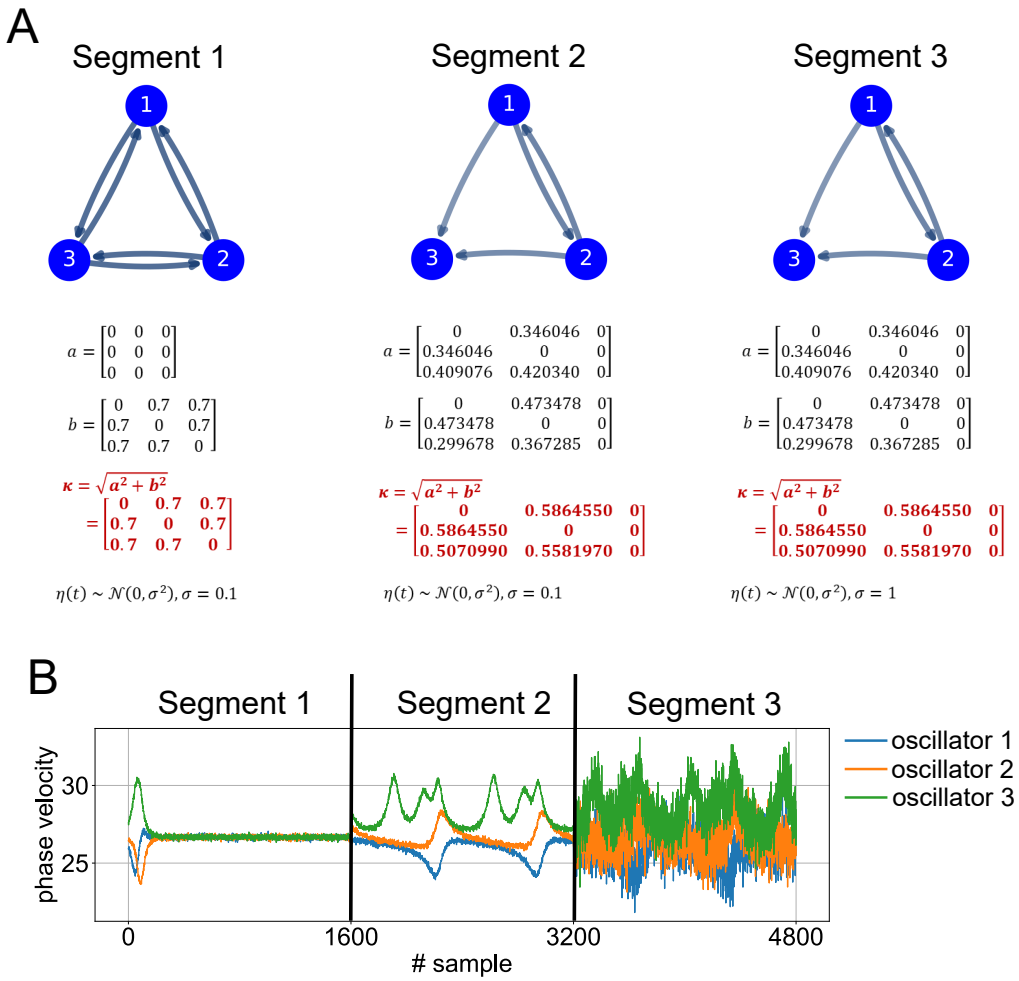

Fig 5. Parameter settings in simulation 3. (A) True network structure and parameter settings in each segment. The time series of synthetic data is generated with the function $\Gamma_{ij}(\theta_j - \theta_i)$ approximated by the 1-st order Fourier series using these parameter settings in each segment. (B) Simulated temporal behavior of the phase oscillator model.

Validation with human scalp EEG data

Next, to confirm the neurophysiological validity, we applied our method to real human EEG data shared by MacFadden et al (2014) [18, 23]. This dataset contained EEG signals that were measured in healthy human participants who were passively listening to 40 Hz amplitude modulated (AM) white noise. In general, when listening to 40 Hz AM white noise, 40 Hz oscillatory activity is recorded in the auditory areas (the so-called auditory steady state response; ASSR) [18, 24–26]). In addition, a recent ASSR study that used a directional connectivity analysis [27] suggested that network connectivity associated with 40Hz ASSR in healthy humans is mainly distributed at central and fronto-temporal areas. The intention of applying our method to the abovementioned open EEG dataset was to confirm whether our method can detect the dynamical changes in neural activity induced by the auditory stimuli.

Open EEG dataset In this dataset, EEGs were recorded with 10-10 system-based 64-channel electrodes (Neuroscan, Inc., North Carolina, USA) in nineteen healthy human participants who were passively listening to 40Hz AM noise or to 40Hz click sounds [18]. The AM noise was binaurally presented through foam insert earphones at 75 dB SPL for 0.5 s with an inter-stimulus interval of 1.0 s [18]. The participants performed over 200 trials of this passive listening task [18]. A more detailed description of the task settings is provided in the original paper [18]. In the following validation, we only used the EEG data of the 40Hz AM noise of participant ID: 1.

Preprocessing EEG signals were off-line re-referenced to the average of the signals from left and right earlobe electrodes. Then, to reduce the effects of eye movement and eye blink signals, we applied an artifact removal method with the empirical mode decomposition (EMD) [28–30]. The detailed description of this EMD-based electrooculographic artifact removal method is provided in previous articles [28, 29]. After removing the artifacts, EEGs were converted to current source density (CSD) signals [31]. To extract phase oscillatory dynamics around 40 Hz, those CSDs were band-pass filtered between 38 and 43 Hz with a zero-phase band-path Butter-worth filter and converted to analytic signals with the Hilbert transform. Next, phase angles were extracted from the analytic signals of the CSDs and divided into epochs with 1.0 s duration form -0.3 s to 0.7 s with a stimulus occurring at 0.0 s. In addition to the above preprocessing, after the epoching of the dataset, reproduce the analysis conditions of the original article for this EEG dataset [18] as much as possible, the epochs that contained amplitudes of raw EEG signals greater than $100\mu V$ were excluded as outliers (this is the same criteria for outlier exclusion than that of McFadden et al (2014) [18]). Out of the recorded trials, 207 trials were accepted and used for the change point detection analysis described in the following section. Moreover, the typical 19 channels (FP1, FP2, F7, F3, Fz, F4, F8, T7, C3, Cz, C4, T8, P7, P3, Pz, P4, P8, O1, and O2) based on the international 10-20 system were used for the following analysis.

Procedures for change point detection After preprocessing, the time series of EEG phases around 40 Hz were applied for the change point detection analysis using our proposed method. The procedure is described below:

- Fit the EEG phase dynamics at 40Hz to the model in Eq (10) with 1st order Fourier series by Bayesian inference (Fig 1)
- Evaluate KL divergence between prior and posterior distributions of the model parameters (i.e., assess the change point score; Fig 2)

- Select the time-sample that has a greater change point score relative to the threshold as the "change point"

Note that the threshold of the change point score is set as mean($\mathrm{KL_{base}}$) + 3SD($\mathrm{KL_{base}}$). The mean($\mathrm{KL_{base}}$) and 3SD($\mathrm{KL_{base}}$) stand for the mean and standard deviation, respectively, of the KL divergence in baseline intervals. Baseline is defined as the immediate pre-stimulus period, which equals to 0.2 s before stimulus onset.

Specifically, we included two conditions for the noise scaling factor σ^2 ($\sigma^2 = 5 \times 10^{-2}$ or $\sigma^2 = 1 \times 10^{-3}$) to compare the detection performance depending on the setting of σ^2. Following the above procedures, the change point detection analysis was applied for each EEG time-series data of a single trial.

Performance evaluation In most cases of the change point detection problems, since the frequency of occurrence of anomaly changes is lower relative to the normal state, the observed samples of each state (i.e., anomaly state or not) are generally imbalanced. In addition, such changes emerge suddenly. Thus, for evaluating the accuracy of change point detection, it is common to define a time-window around the true change point to allow for minor delays of change point detection [32, 33]. Besides, considering the results of the time-frequency analysis performed in the original article of the open EEG dataset that we used, the time-frequency representation of EEGs related to 40 Hz ASSR appeared with a delay time of 0.1 s [18]. Given the abovementioned, to permit a minor delay in neuronal response, we defined the "error tolerance area" as 0.1 s periods after the true time-point of stimulus on/off-set as shown in Fig 6. The time-points of the change point score are labeled as shown in Fig 6 B – E. If a significant increase in the change point score is detected within the error tolerance area, all of the time-points corresponding to this window are labeled as True Positive (TP) (Fig 6B). In contrast, if no change detection is observed within the error tolerance area, all of the time-points corresponding to this window are labeled as False negative (FN) (Fig 6E). Regarding time-points in outside of the error tolerance area, time-points with no detection are labeled as True negative (TN) (Fig 6C), and time points with detection are labeled as False Positive (FP) (Fig 6 D).

Moreover, considering the issue of performance evaluation with imbalanced data in the classification problem, we used the following three indices of detection accuracy [34], and accuracy was calculated for each trial.

$$
\begin{aligned}
\text{Accuracy} &= \frac{\mathrm{TP}+\mathrm{TN}}{\mathrm{TP}+\mathrm{FP}+\mathrm{FN}+\mathrm{TN}} \\
\mathrm{F_1}\ \text{measure} &= \frac{2\mathrm{TP}}{2\mathrm{TP}+\mathrm{FP}+\mathrm{FN}} = \frac{2\cdot\text{precision}+\times\text{recall}}{\text{precision}+\text{recall}} \\
\text{G mean} &= \sqrt{\left(\frac{\mathrm{TP}}{\mathrm{TP}+\mathrm{FP}}\right)\times\left(\frac{\mathrm{TN}}{\mathrm{TN}+\mathrm{FP}}\right)} = \sqrt{\text{precision}\times\text{recall}} \\
\text{where,}\quad \text{precision} &= \frac{\mathrm{TP}}{\mathrm{TP}+\mathrm{FP}},\quad \text{recall} = \frac{\mathrm{TP}}{\mathrm{TP}+\mathrm{FN}}
\end{aligned}
\tag{18}
$$

In this analysis, the abovementioned accuracy metrics were assessed from 0.0 to 0.6 s intervals for each trial. Baseline intervals from which data were used to calculate the threshold of the change point score were excluded from this evaluation.

To evaluate the statistical significance of the detection accuracy, the median values of each index over all trials were calculated and the significance of these median values was assessed with a one-tailed permutation test. The null distribution of each index for the permutation test was generated in the following manner:

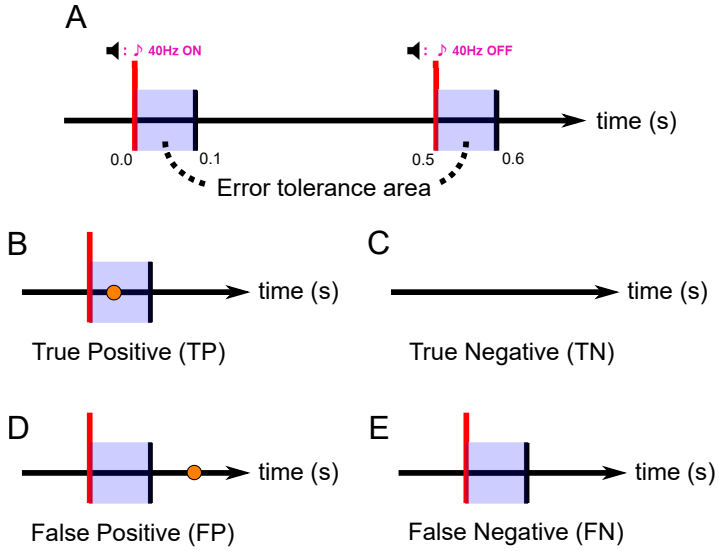

Fig 6. Schematic depiction of the change point evaluation. (A) Schematic depiction of the time protocol of stimulus on/off-set and definition of the error tolerance area. The red vertical lines indicate stimuli on/off-set. The blue shaded areas and the black vertical lines indicate the error tolerance area. (B-E) Relevant situations for the evaluation for the detected change points. If the change point is detected within the error tolerance area, time samples within the time window are labeled as True Positive (B). See text for details.

1. The true labels of each time sample (positive or negative) are shuffled. (Note that positive and negative labels before shuffling are defined as the time samples corresponding inside and outside of the error tolerance area, respectively.)
2. The detection accuracy with each index is calculated with randomized labels for each trial.
3. The randomized median score of all trials is calculated for each index.
4. The abovementioned steps 1 to 3 are repetitively executed 1000 times, and the null distribution of each evaluation index is generated from those 1000 randomized median scores.

For this statistical analysis, we used the null distribution generated with the above procedure to estimate the threshold ($p = 0.05$). To account for the effects of multiple comparison, the results of the statistical test were corrected using the Bonferroni method [35].

Results

Result of synthetic data

To examine whether our proposed method can detect the occurrence of changes in dynamical structures of the network, we first conducted the three simulations with synthetic data.

Simulation 1

The results of simulation 1 are shown in Fig 7, 8 and 9. In Fig 7, the red dots, which indicate the significance of the change point score, are located around the starting points of segment 1 and segment 2 (indicated as "Structural change" in Fig 7). Furthermore, it is remarkable that significant change point scores were not detected around the boundary between segments 2 and 3 (indicated as "Noise-level change" in Fig 7). Thus, we confirmed that the change points (indicated by the red dots) were correctly detected only in the case of timing of the "Structural changes".

In addition, to further examine whether our proposed method could detect the time-evolving dynamics of oscillatory networks, we attempted to visualize network couplings and phase coupling functions for each segment. Fig 8 shows the comparison between the true and predicted dynamical structures of the network for each segment. The predicted networks were visualized by calculating the median of the coupling strength in Eq (11) with estimated Fourier coefficients for each segment. As shown in this figure, true and estimated networks were very similar. Especially, in Segment 1, even though it is the typical situation where spurious correlations between the 1st and 2nd oscillators would easily occur caused by the common drive from the 3rd oscillator as a confounder, our method was able to detect network coupling correctly. Based on this result, we would like to emphasize that model-based network analysis is an efficient approach to reduce the false detection of network coupling caused by spurious correlations.

In addition to the abovementioned, Fig 9 shows the phase coupling function predicted by our proposed method. The averaged phase coupling function was evaluated as the median of the $\Gamma_{ij}\left(\theta_j(t) - \theta_i(t)\right)$ with estimated Fourier coefficients for each segment. If the interaction between i and j th oscillators does not exist, the function $\Gamma_{ij}\left(\theta_j(t) - \theta_i(t)\right)$ will be flat, indicating no interaction between the two oscillators. As shown in Fig 9 A, our model estimated so that the function $\Gamma_{ij}\left(\theta_j(t) - \theta_i(t)\right)$ would be flat in the case of no interaction between the pair of oscillators. Moreover, as can be seen in Fig 9 B and C, even though the noise-level was quite different between segments 2 and 3, the predicted phase coupling functions were similar between these two segments. This indicates that our method could capture the changes in the phase coupling function as well as in network coupling.

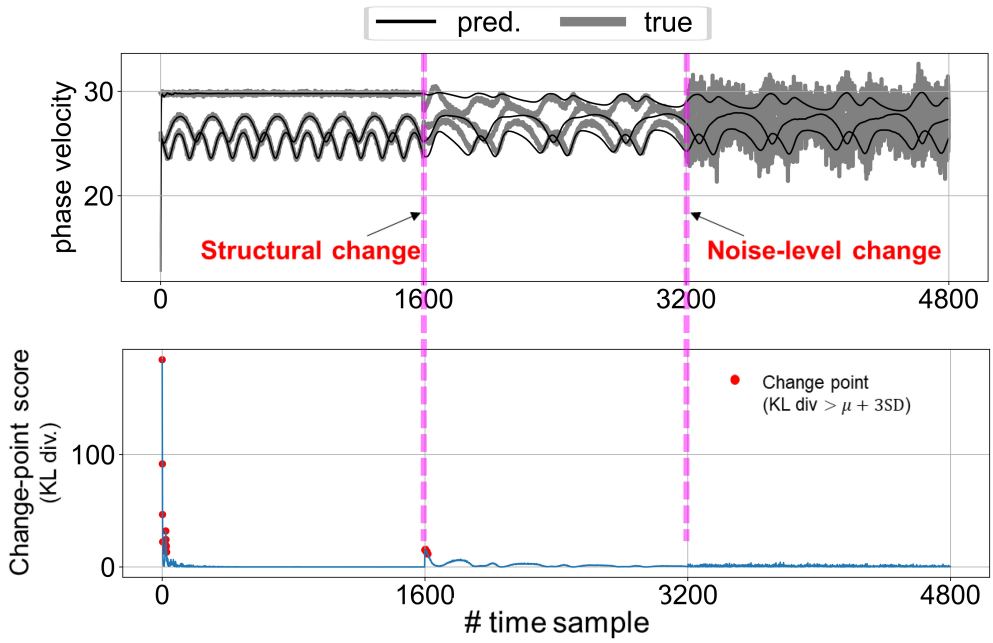

Fig 7. Results of change point detection in simulation 1. The upper panel indicates the time course of the estimated behavior of the phase oscillator model. The black lines and the gray bold lines show the predicted and the true behavior of the function, respectively. The lower panel indicates the time course of the change point scores. The red dots indicate the selected change points based on the pre-defined threshold. The pink vertical dashed lines show the first and second event (i.e. structural and noise level change point).

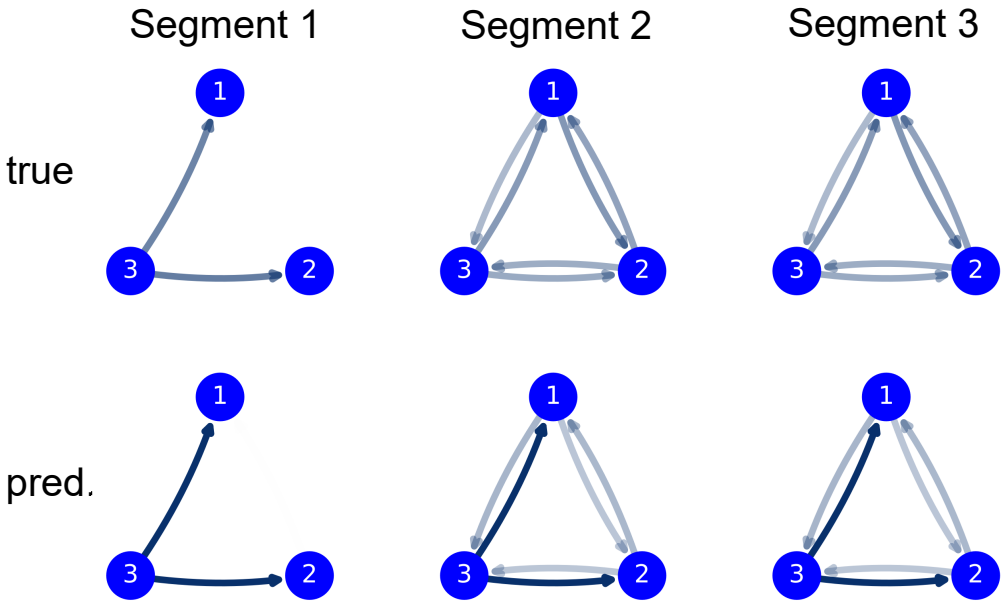

Fig 8. Comparison of true and predicted network structures in simulation 1. The upper panel shows the true network structure in each segment. The lower panel shows the predicted network structure in each segment. The predicted network structure was evaluated as the average of the estimated values in Ep (11) for each segment.

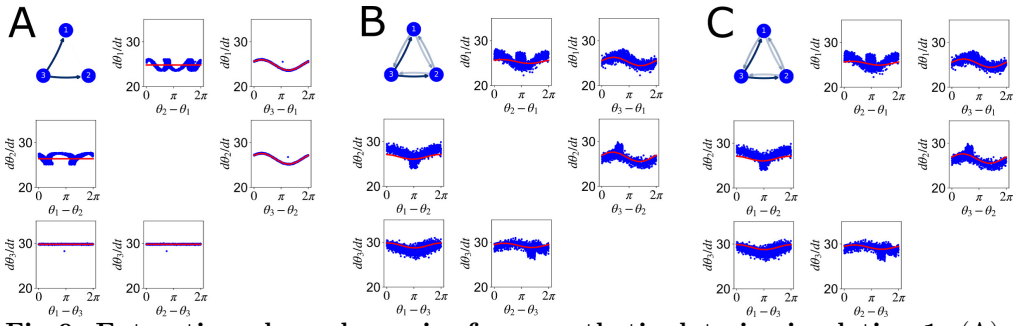

Fig 9. Extracting phase dynamics from synthetic data in simulation 1. (A) Estimated phase coupling function in segment 1. (B) Estimated phase coupling function in segment 2. (C) Estimated phase coupling function in segment 3. The upper left diagram in each panel indicates the predicted network structure. The blue dots show the actual samples of phase time-series data for all oscillators. The red lines are the averaged phase response curves estimated by our proposed method in each segment. The phase coupling function would be flat if the interaction between i and j th oscillators did not exist.

Simulation 2

The results of simulation 2 are shown in Fig 10, 11 and 12. Equally to the indicated by the results of simulation 1, we confirmed that our method could correctly detect the occurrence of structural changes in the model parameters. In Fig 10, the selected change points (i.e. time-points where the change point score is greater than the threshold) are located around the starting point of segments 1 and 2, whereas no change points are detected in segment 3. Moreover, although the predicted model parameters identified the tendency of coupling strength being relatively greater than the true coupling (Fig 11), the estimated phase coupling function did precisely capture the trend of the synthetic data (see the red curve and the blue dots in Fig 12).

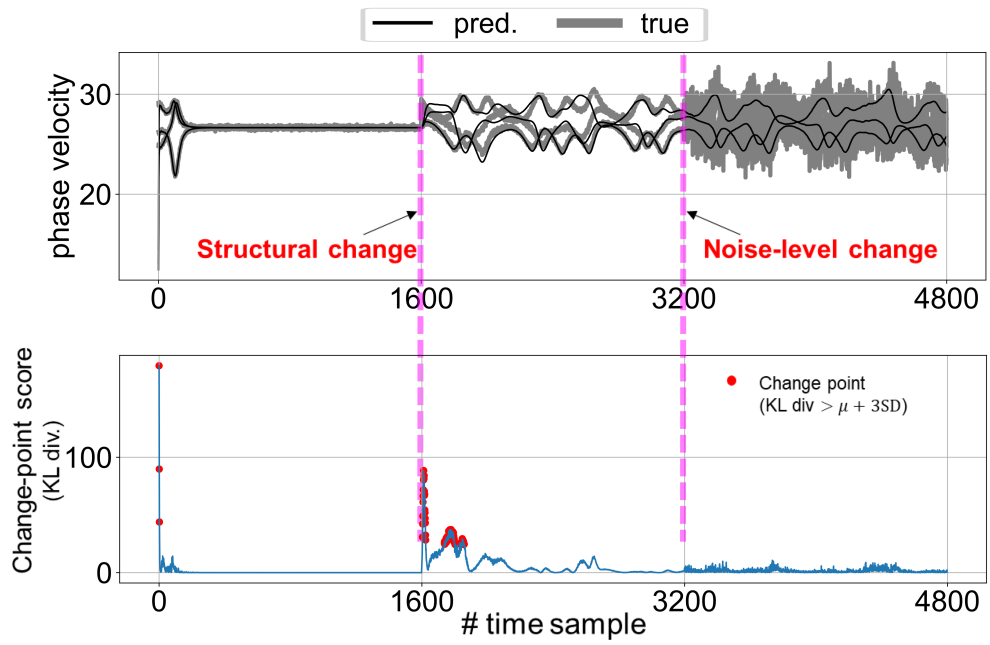

Fig 10. Results of change point detection in simulation 2. The upper panel indicates the time course of the estimated behavior of the phase oscillator model. The black lines and the gray bold lines show the predicted and true behavior of the coupled oscillators, respectively. The lower panel indicates the time course of change point scores. The red dots represent the selected change points based on the pre-defined threshold. The pink vertical dashed lines show the first and second events (i.e. structural and noise level change points).

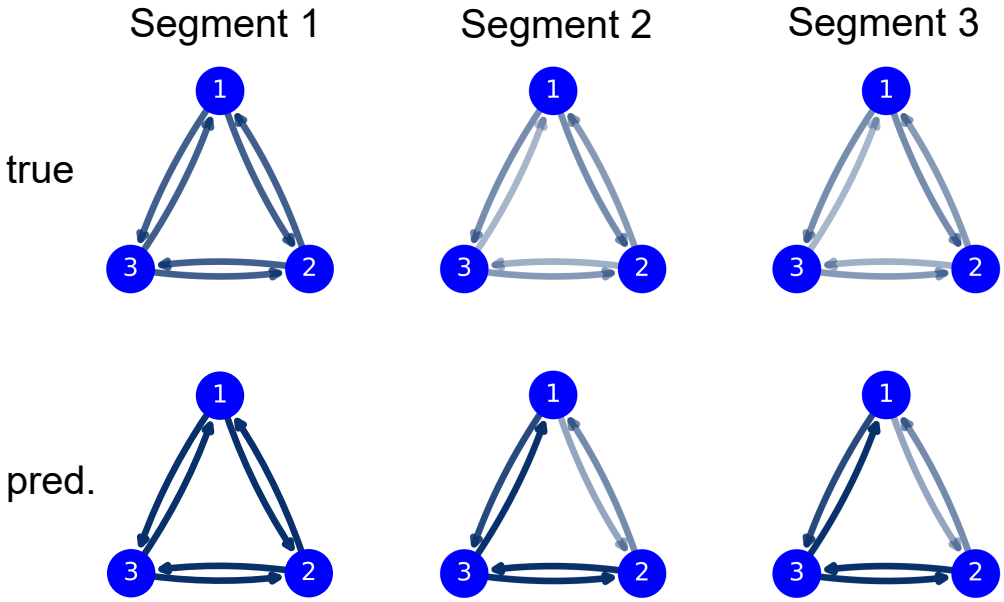

Fig 11. Comparison of true and predicted network structures in simulation 2. The upper panel shows the true network structure in each segment. The lower panel shows the predicted network structure in each segment. The predicted network structure was evaluated as the average of the estimated values in Ep (11) for each segment.

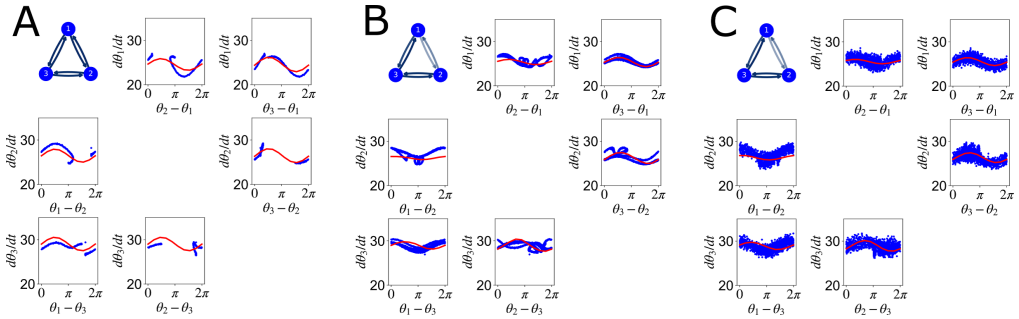

Fig 12. Extracting phase dynamics from synthetic data in simulation 2. (A) Estimated phase coupling function in segment 1. (B) Estimated phase coupling function in segment 2. (C) Estimated phase coupling function in segment 3. The upper left diagram in each panel indicates the predicted network structure. The blue dots show the actual samples of phase time-series data in each oscillator. The red lines are the averaged phase response curves estimated by our proposed method in each segment.

Simulation 3

The results of simulation 3 are shown in Fig 13, 14 and 15. Fig 13 suggests that no significant change point scores were detected in segment 3 (Fig 13), Moreover, we confirmed that our method could correctly detect the occurrence of structural changes of the networks, equally to the performance with other simulation settings. However, the prediction of the network structures are little bits of different against the true ones in segment 2 and 3 (Fig 14). The reason for such differences could be the effect of perfect phase locking. As shown in Fig 4A and Fig 5A, the parameter settings of segment 1 in simulation 3 were the same as in simulation 2, and the phase dynamics for each oscillator in segment 1 was perfectly synchronized in both simulations. In contrast, the interactions between oscillators in segment 2 were asymmetric in simulation 3, while they were symmetric in simulation 2. Even though the results suggest that our method correctly detected the change points around the starting point of segment 2 in both simulation 2 and simulation 3 (Fig 10 and 13), the prediction error of the network structure appeared only in segment 2 of simulation 3 (Fig 14).

However, despite the prediction error, our results indicate that the proposed method could detect the structural changes of the network parameters accurately independently of the simulation settings (Fig 7, 10, and 13). It should be noted that in simulation 3, the estimated phase coupling function seemed to be accurately fitted to the time series of synthetic data as shown in Fig 15.

To summarize the results of these three simulations, our method could detect the changes in dynamical structures of the networks regardless of whether observation noise was added to the time-series data.

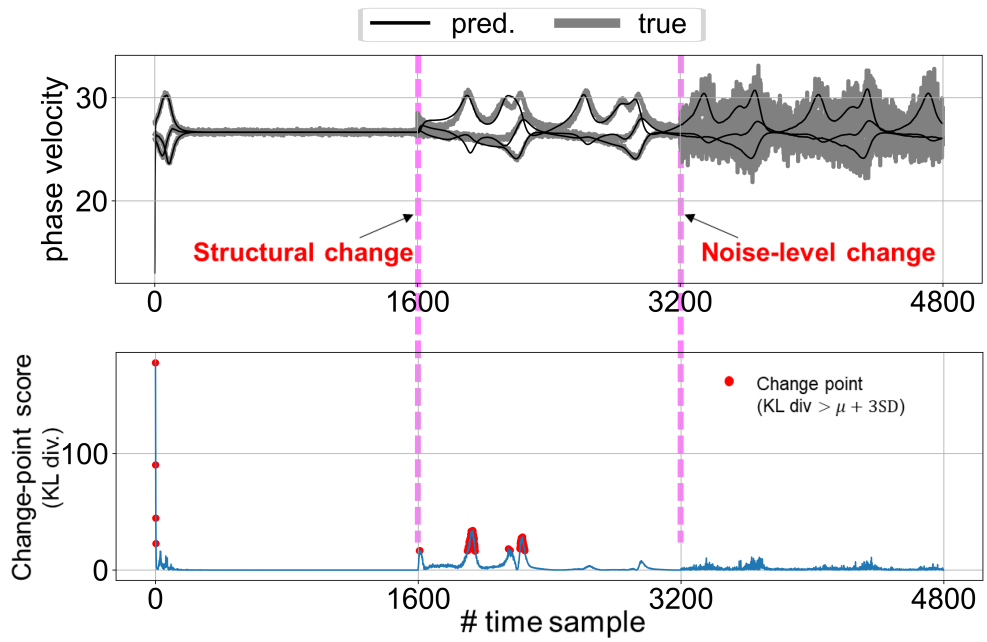

Fig 13. Result of change point detection in simulation 3. The upper panel indicates the time course of the estimated behavior of the phase oscillator model. The black lines and the gray bold lines show the predicted and true behavior of the function, respectively. The lower panel indicates the time course of change point scores. The red dots represent the selected change points based on the pre-defined threshold. The pink vertical dashed lines show the first and second event (i.e. structural and noise level change point).

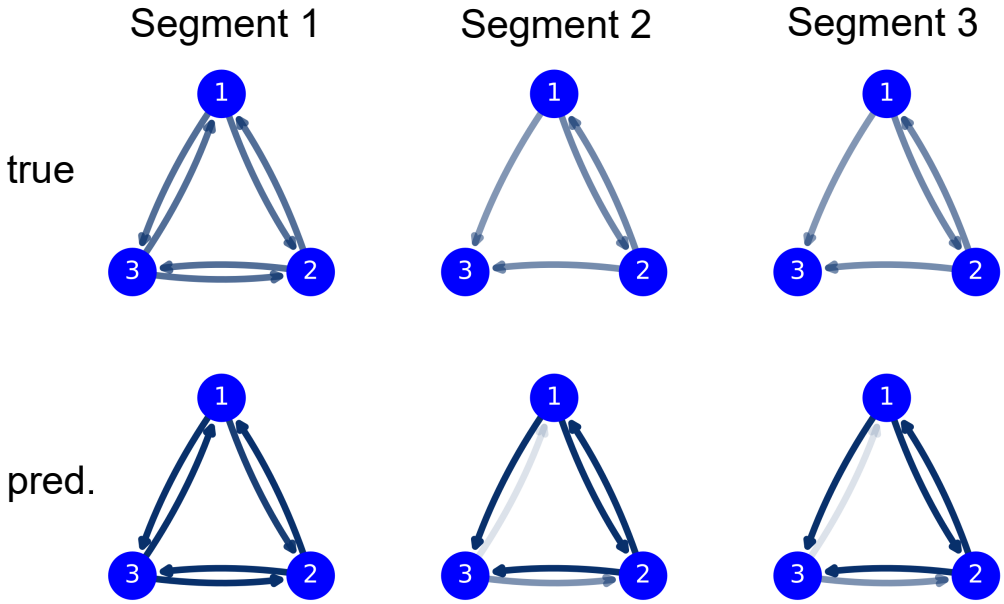

Fig 14. Comparison of true and predicted network structures in simulation 3. The upper panel shows the true network structure in each segment. The lower panel shows the predicted network structure in each segment. The predicted network structure was evaluated as the average of the estimated values in Ep (11) for each segment.

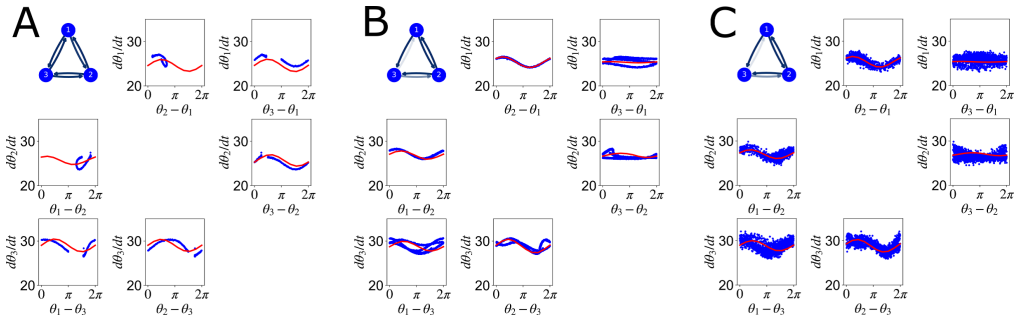

Fig 15. Extracting phase dynamics from synthetic data in simulation 3. (A) Estimated phase coupling function in segment 1. (B) Estimated phase coupling function in segment 2. (C) Estimated phase coupling function in segment 3. The upper left diagram in each panel indicates the predicted network structure. The blue dots show the actual samples of phase time-series data in each oscillator. The red lines are averaged phase response curves estimated by our proposed method in each segment.

Results of scalp EEG data

Next, by applying our proposed method on open EEG data shared by McFadden et all (2014) [18], we evaluated the neurophysiological validity of our method. Moreover, since the effect of the free parameter σ^2, which is a noise scaling factor of the model prediction, is present in our method, we compared the accuracy of change point detection with two different settings of σ^2.

Fig 16 shows the typical results from Subject 1. In this figure, it is depicted how the change point score is significantly increased around the stimulus on-set and off-set in both settings of σ^2, although the temporal behavior of the score is more sensitive to a decrease in σ^2. This tendency is also reflected in the detection accuracy as shown in Table 1. Even though the averaged accuracy of change point detection is significantly higher than the chance level in both settings of σ^2 for each evaluation index, all scores were relatively higher in $\sigma^2 = 0.05$ compared to $\sigma^2 = 0.001$. In the case of $\sigma^2 = 0.05$, our method could detect the on/off-set with around 74 % accuracy (Table 1). Considering the context of Bayesian regression, the precision of model fitting would be related with a decrease in σ^2 in Eq (16), but this also means that extremely small values of σ^2 lead to overfitting (see the detailed description in the Discussion section). Therefore, the results indicate that accuracy of model fitting and change point detection have a trade-off relationship.

Table 1. Change point detection in EEGs. The value of each element represents the median score value across all trials for each evaluation index. The asterisk * indicates the statistical significance of each evaluation index ($p < 0.01$ with Bonferroni correction).

	Noise scaling factor σ^2	
	$\sigma^2 = 0.05$	$\sigma^2 = 0.001$
Accuracy	0.7383*	0.7100*
F1-measure	0.6591*	0.6280*
G-mean	0.6575*	0.6388*

To further assess the details of connectivity changes, the estimated couplings for each pair of EEG channels during task periods were compared with those in the immediate pre-stimulus period, which corresponds to a 0.2 s interval before stimulus onset. In this analysis, task periods were defined as the interval between the detected on-set and the detected off-set of the auditory stimulus based on the change point score, and such intervals were assessed as time-points of significant change point score located the nearest to time-points of true on/off-set. Fig 17 shows a typical example of this comparison (trial 115, Subject 1). As shown in the right panel of Fig 17 A and B, the coupling strength in the temporal-frontal (T8–Fz, FP2), the temporal-central (T8-C3), and the temporal-parietal (T8–Pz) areas increased during task periods, relative to baseline periods. In addition, the coupling in the parieto-frontal area (including Fz to Pz, and P3 to F3) also increased during task periods. This tendency is consistent with the results of a previous study on the directional connectivity of ASSR reflected in human scalp EEGs [27]. Moreover, these connectivity patterns were identified as a common tendency in trials in which there was a higher accuracy of detection of stimulus on/off-set in our analysis.

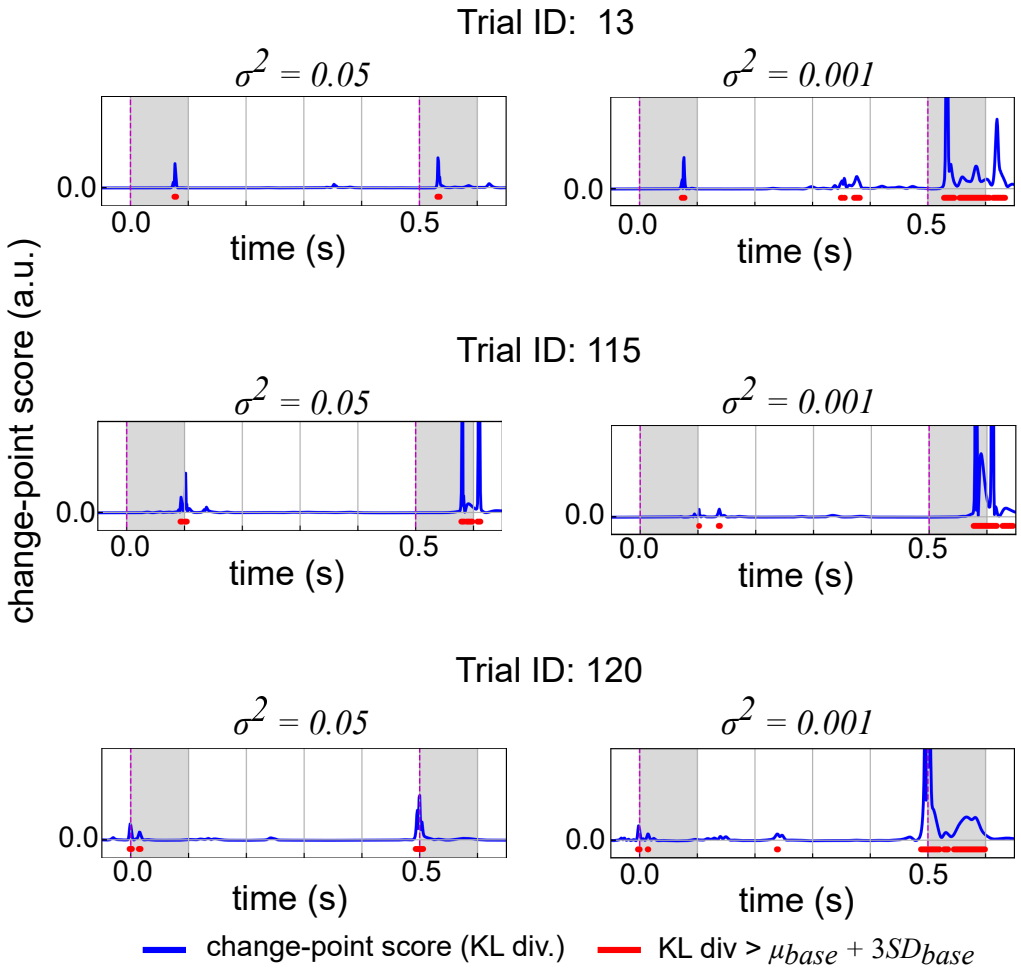

Fig 16. Typical good results in change point detection on EEG data for each condition of σ^2. The pink vertical dashed lines and the gray shaded areas indicate the on-set/off-set of stimuli and the error tolerance area, respectively.

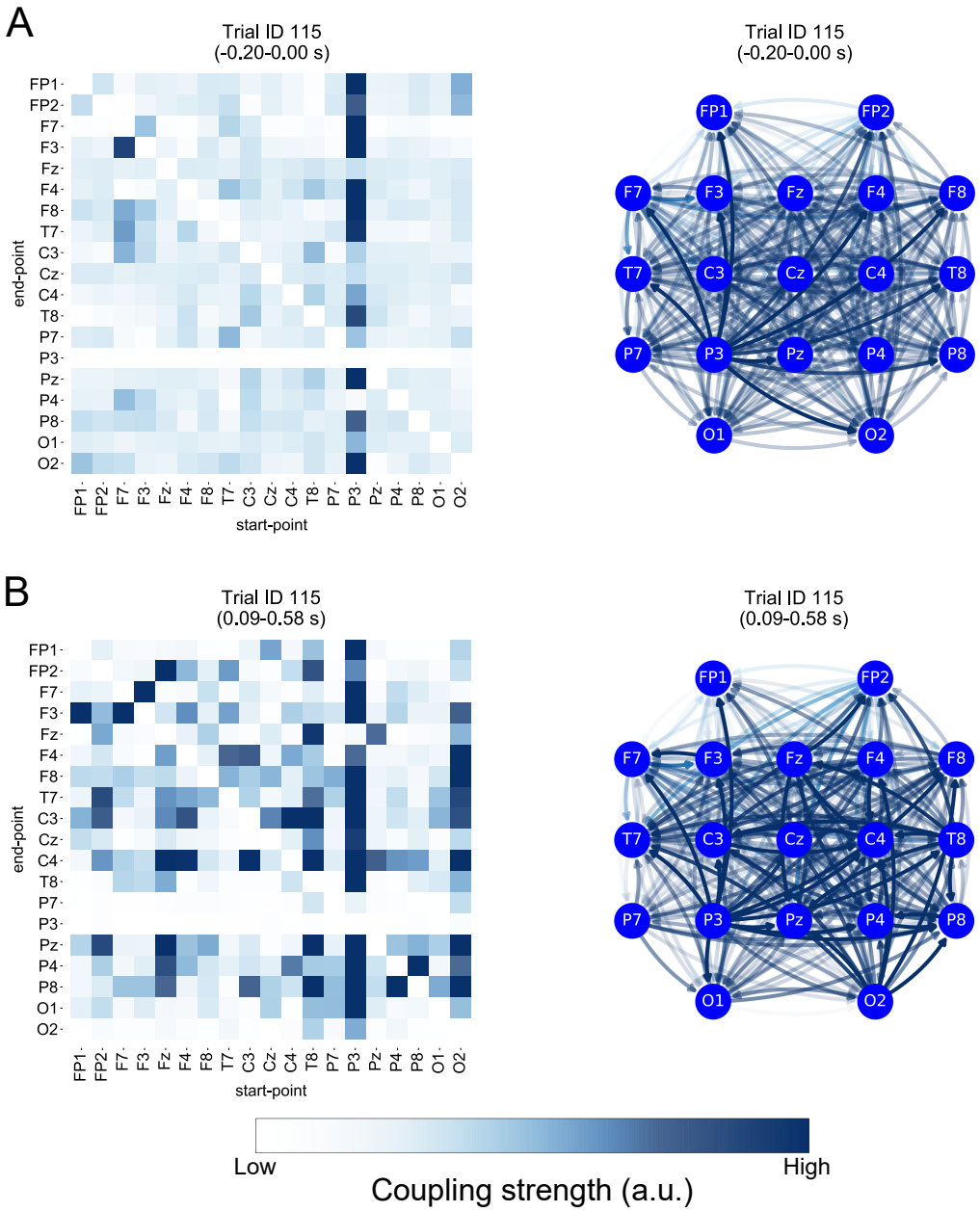

Fig 17. Representative single-trial network estimation from the EEG data (trial ID: 115, $\sigma^2 = 0.05$). (A) The left panel indicates estimated phase coupling strength, which is averaged from the baseline period ($-0.20 - 0.00$ s). The right panel indicates the phase coupling for each pair of EEG sensors corresponding to the left panel in (A). (B) The left panel indicates estimated phase coupling strength, which is averaged from the intervals between two detected change points corresponding to the stimulus on-set/off-set ($0.09 - 0.58$ s). The right panel indicates the phase coupling for each pair of EEG sensors corresponding to the left panel in (B).

Discussion

In this study, we proposed a new approach to detect the change points of brain networks by extending the data-driven method to estimate phase oscillatory dynamics based on sequential Bayesian inference. To validate our proposed method, we applied it to numerical and empirical neurophysiological data. Regarding the results of the evaluation with numerical data, we confirmed that the change point score of our method significantly increases only when structural changes in the dynamical network occur, and not when noise-level changes in the dynamical network occur. The results support two assumptions for our proposed method: (1) time-evolving dynamics and data structures of the functional brain networks can be represented by a coupled phase oscillator model, and (2) temporal changes in the dynamical structures of the brain are reflected in changes in model parameters. Furthermore, according to the results of the evaluation with neurophysiological data, our method was able to detect the change point of phase oscillatory dynamics induced by auditory stimuli with around 74 % accuracy on average. These findings suggest that our proposed method has mathematical and neurophysiological validity. In the following section, we discuss the neuroscientific significance of our proposed method, comparing our results with evidence from previous studies on time-varying functional connectivity analysis.

Advantages of our proposed method

The originality of our proposed method lies in applying sequential Bayesian inference to estimate the phase coupling function of dynamical networks. Using this approach, the current state of the network dynamics of the brain could be expressed as a probability distribution (Fig 2). Therefore, our method can not only visualize the time-varying network couplings of the brain, but also represent the occurrence of the changes in dynamical structures of the brain with a quantitative index (i.e. KL divergence).

Relevant previous studies have reported three types of methods to estimate the temporal changes in functional connectivity of the human brain. The first type of methods are related to dynamic functional connectivity (DFC) [9, 10]. The studies on this type of methods extend the conventional functional connectivity analysis to estimate time-varying network structures by applying the sliding window method [9, 10]. Even though DFC is proposed to focus on the time-evolving dynamics of brain networks, this method evaluates functional networks with static indices, such as the correlation between time-series data, for each time window separately. Thus, these studies do not explicitly consider the time-evolving dynamics of the time-series data, because multivariate time -series with non-stationary dynamics usually contain temporal dependence, as in the Markov process. Moreover, in most of the studies that use DFC, when evaluating the networks at each time window, the coupling strength for each pair of brain areas is assessed based on the temporal correlation with the time-series data. According to the evidence presented by an economic study [11], correlation coefficients between two different time-series data tend to be large regardless of the existence of causality between the two time-series data (i.e., spurious correlation). Therefore, considering these issues, the resulting network structure based on DFC could lead to an incorrect interpretation caused by spurious correlations between time-series data.

The second type of methods is the change point detection based on dynamic connectivity regression (DCR) [36, 37]. TDCR is similar to our method in that it is based on the framework of anomaly detection based on probability distributions. However, it is different in that network couplings of the brain are estimated with a graphical lasso. A graphical lasso is an algorithm that estimates undirected graphs based on the multivariate Gaussian distribution with sparse prior of covariance matrix [36–38]. Thus, this method estimates network structures assuming a linear

interaction between signals from multiple brain areas using the inverse covariance matrix of the multivariate Gaussian distribution. Therefore, this method cannot capture the nonlinear dynamical structure of brain networks. Within the context of the study of dynamical systems with computational neuroscience, inter-regional interactions and temporal behavior of the brain activity should be considered as nonlinear systems [1–4].

The third type of methods studies the time-varying functional connectivity [39] on the basis of the Hidden Markov model (HMM). Unlike the abovementioned methods, the HMM-based approach is more advanced in the estimation of time-varying functional connectivity because it considers the time-evolving dynamics. The HMM assumes that the time-evolving dynamics of the time-series data can be modeled as a probabilistic state transition of hidden-state variables by applying the Markov-chain algorithm. In the framework of the HMM, the temporal dynamics of the data are explained based on the state transition of the hidden variables in the model at time $t+1$ conditioned by the probability of the state of the hidden variables at time t. All state transition probabilities of the whole time -series can be parameterized by the state-transition matrix. By the prior learning of model parameters (containing the state-transition matrix) with training data, the HMM can be used for the detection of state changes of unknown time-series data. However, the parameter space in this model increases exponentially according to the number of hidden processes that equal time samples in the time-series data. In other words, since a large data set is required to learn the state transition matrix in order to satisfy the accurate forecasting of unknown data, reliability for detecting state-changes directly depends on data size, variability, and quality of the dataset. Moreover, another study on the forecasting of change points of time-series data [40] suggested that a method based on sequential Bayesian inference is more reliable for the prediction of time -series than a method based on the HMM.

Compared with the abovementioned studies [9, 10, 36, 37, 39] , our proposed method is advanced in the following two points. First, our method considers both the time-evolving dynamics and a nonlinear dynamical structure of functional brain networks. Unlike the framework of DFC and DCR, our method adequately considers nonlinear and time-evolving properties of the dynamical brain activity by applying a model-based approach to estimate functional brain networks. The advantage of a model-based approach such as the one proposed in our method lies in that the misinterpretation caused by spurious correlations is largely reduced by assuming a network system with temporal dynamics based on certain models. As we mentioned in the results of simulation 1, our method was able to detect network coupling in this segment correctly, even in situations where conventional correlation-based functional connectivity analysis (such as DFC) would typically lead to spurious correlations (see Fig 8). This is supporting evidence for the above-mentioned advantage of our model-based analysis approach. Second, our method can sequentially detect changes in dynamical structures of the brain based on Bayesian inference. Our method is more advanced in that prior learning with large datasets is not required, as is the case with the HMM-based method. Although our approach does not directly model the temporal dependence in non-stationary time -series explained by the sequential Markov chain as does the HMM-based model, our method can consequently consider the temporal dynamics of the time-series data by applying sequential Bayesian inference to estimate the time-varying model parameters. Moreover, as a subsidiary advantage of applying the coupled phase oscillator model to estimate the network dynamics of the brain, directional network couplings could be detected, unlike with the HMM-based method or with DFC and DCR.

In summary, by assuming the property of time-evolving dynamics in the observed data based on a dynamical model, the proposed method succeeded in providing a quantitative interpretation of the functional role of network dynamics in the brain.

Neuroscientific interpretation and generalizability

In this study, by assuming the coupled phase oscillator model as the representation of the time-evolving dynamics of functional brain networks, we expected the changes of functional brain networks to be quantified as changes in dynamical structures of the model parameters. As a result, our method can successfully detect changes in dynamical structures when the changes occur in dynamical structures of the network, and this is not affected by changes in observation noise level. This indicates that the model-based approach to detecting the change point of functional brain networks would rather be convenient to interpret the temporal dynamics of the brain.

Another remarkable point of our presented study is that our method can visualize the dynamical structures reflected in scalp EEGs on a single trial basis. In this study, we applied our method on a multi-channel time -series of human scalp EEG that were measured from a healthy human participant while passively listening to 40Hz AM noise [18, 23]. In general, when listening to 40 Hz AM noise, a broad area of EEG signals is synchronized around 40 Hz. [18, 24–26]). A recent ASSR study using connectivity analysis [27] suggested that network connections reflected in EEGs are mainly distributed at the centro-frontal, the parieto-occipital, and the fronto-temporal areas. These findings are consistent with our results as shown in Fig 17B. Taken together, our proposed method successfully detected the neuroscientifically relevant dynamics on ASSR from single trial EEGs.

In summary, our provided method was successful in assessing the dynamical structures of the brain as well as the change points of those dynamical structures. Since neuroscientists are becoming interested in the relationship between flexible changes in functional brain networks and cognitive functions [5–9], our method could help to reveal the crucial role of flexible changes in dynamical structures of the brain.

Limitations of this study

However, even though our proposed method has some advantages, as mentioned above, the expressive power of phase dynamics in our method is strongly dependent on the pre-defined function of the dynamical model. In our method, since the phase dynamics are approximated by the Fourier series, prediction performance and reliability depend on the dimension of the Fourier series. This is one of the reasons why the detection accuracy was around 74% on average even in the case of best performance; we can consider this as a limitation of our proposed method. In addition, we found that detection accuracy tends to decrease slightly with a decrease in the noise scaling factor σ^2 (Table 1). As we can see in Eq (16), the parameter σ^2 affects the noise factor η in the model. Because $\mathbf{f}\Sigma_{\mathrm{K}}\mathbf{f}^T$, which is the first term of the right-hand side of the Eq (16), tends to be around zero throughout the sequential update of the predictive distributions, η converges with $\sigma^2 I$. This tendency directly influences the variance of the fitting error of the model. Therefore, the reason for the difference in detection accuracy depending on σ^2 could be considered as the effect of excessive sensitivity of the change point score caused by the overfitting caused by the extremely small value of σ^2. Considering these, both the parameters of the dimension of the Fourier series and σ^2 affect the performance of change point detection. However, these parameters should be selected exploratorily, since the optimal setting for each parameter depends on the complexity and dimensionality of the data.

IDespite these limitations, our method provides advantages against the conventional methods in that both the visualization of the network structure and the detection of the change point are simultaneously estimated based on Bayesian inference. Further studies that consider the method of change point detection without assuming the model equations (e.g., applying the non-parametric dynamical modeling with Gaussian

process [40–42]) are needed.

Conclusions

In this study, we provided a new method for detecting the changes in dynamical structures of the brain. By applying our proposed method on numerical and electroencephalographic data, we confirmed that our proposed method successfully detects the change points where dynamical changes of the network occur. These results suggest that our proposed method could help to reveal the neural basis of the dynamical changes of functional brain networks. To apply our proposed method in future neuroscience studies, further studies are required with a model-free approach to change point detection of the brain network dynamics.

Acknowledgments

This research was supported in part by the JSPS KAKENHI (20K19867) and by the Encouraging Grants for Young Researchers at National Institute for Physiological Sciences.

References

1. Breakspear M, Heitmann S, Daffertshofer A. Generative models of cortical oscillations: neurobiological implications of the kuramoto model. Frontiers in Human Neuroscience. 2010;4(November):1–14. doi:10.3389/fnhum.2010.00190.

2. Cabral J, Hugues E, Sporns O, Deco G. Role of local network oscillations in resting-state functional connectivity. NeuroImage. 2011;57(1):130–139. doi:10.1016/j.neuroimage.2011.04.010.

3. Deco G, Kringelbach ML, Jirsa VK, Ritter P. The dynamics of resting fluctuations in the brain: metastability and its dynamical cortical core. Scientific Reports. 2017;7(1):1–14. doi:10.1038/s41598-017-03073-5.

4. Deco G, Cabral J, Woolrich MW, Stevner ABA, van Hartevelt TJ, Kringelbach ML. Single or multiple frequency generators in on-going brain activity: a mechanistic whole-brain model of empirical MEG data. NeuroImage. 2017;152:538–550. doi:10.1016/j.neuroimage.2017.03.023.

5. Bassett DS, Wymbs NF, Porter MA, Mucha PJ, Carlson JM, Grafton ST. Dynamic reconfiguration of human brain networks during learning. Proceedings of the National Academy of Sciences of the United States of America. 2011;108(18):7641–7646. doi:10.1073/pnas.1018985108.

6. Baum GL, Ciric R, Roalf DR, Betzel RF, Moore TM, Shinohara RT, et al. Modular Segregation of structural brain networks supports the development of executive function in youth. Current Biology. 2017;27(11):1561–1572.e8. doi:10.1016/j.cub.2017.04.051.

7. Braun U, Schäfer A, Walter H, Erk S, Romanczuk-Seiferth N, Haddad L, et al. Dynamic reconfiguration of frontal brain networks during executive cognition in humans. Proceedings of the National Academy of Sciences of the United States of America. 2015;112(37):11678–11683. doi:10.1073/pnas.1422487112.

8. Braun U, Schäfer A, Bassett DS, Rausch F, Schweiger JI, Bilek E, et al. Dynamic brain network reconfiguration as a potential schizophrenia genetic risk mechanism modulated by NMDA receptor function. Proceedings of the National Academy of Sciences of the United States of America. 2016;113(44):12568–12573. doi:10.1073/pnas.1608819113.

9. Hutchison RM, Womelsdorf T, Allen EA, Bandettini PA, Calhoun VD, Corbetta M, et al. Dynamic functional connectivity: promise, issues, and interpretations. NeuroImage. 2013;80:360–378. doi:10.1016/j.neuroimage.2013.05.079.

10. Damaraju E, Allen EA, Belger A, Ford JM, McEwen S, Mathalon DH, et al. Dynamic functional connectivity analysis reveals transient states of dysconnectivity in schizophrenia. NeuroImage: Clinical. 2014;5(July):298–308. doi:10.1016/j.nicl.2014.07.003.

11. Granger CW, Newbold P, Econom J. Spurious regressions in econometrics. Baltagi, Badi H A Companion of Theoretical Econometrics. 1974;2:557–61. doi:10.1016/0304-4076(74)90034-7.

12. Netoff T, Schwemmer MA, Lewis TJ. Phase response curves in neuroscience; 2012. Available from: `http://link.springer.com/10.1007/978-1-4614-0739-3`.

13. Ota K, Aoyagi T. Direct extraction of phase dynamics from fluctuating rhythmic data based on a bayesian approach; 2014.

14. Suzuki K, Aoyagi T, Kitano K. Bayesian estimation of phase dynamics based on partially sampled spikes generated by realistic model neurons. Frontiers in Computational Neuroscience. 2018;11(January):1–13. doi:10.3389/fncom.2017.00116.

15. Onojima T, Goto T, Mizuhara H, Aoyagi T. A dynamical systems approach for estimating phase interactions between rhythms of different frequencies from experimental data. PLoS Computational Biology. 2018; p. 1–20. doi:10.1371/journal.pcbi.1005928.

16. Sarris AH. A bayesian approach to estimation of time-varying regression coefficients. Journal of economic and social measurement. 1973;2(4):501–523.

17. Bishop CM. Pattern recognition and machine learning (Information science and statistics). 1st ed. Springer; 2007.

18. McFadden KL, Steinmetz SE, Carroll AM, Simon ST, Wallace A, Rojas DC. Test-retest reliability of the 40 Hz EEG auditory steady-state response. PLoS ONE. 2014;9(1):59–61. doi:10.1371/journal.pone.0085748.

19. Kuramoto Y. Chemical oscillations, waves, and turbulence. Springer; 1984. Available from: `hhttps://www.springer.com/gp/book/9783642696916`.

20. Ko TW, Ermentrout GB. Phase-response curves of coupled oscillators. Physical Review E. 2009;79(1):016211. doi:10.1103/PhysRevE.79.016211.

21. Stankovski T, Pereira T, McClintock PVE, Stefanovska A. Coupling functions: universal insights into dynamical interaction mechanisms. Reviews of Modern Physics. 2017;89(4):045001. doi:10.1103/RevModPhys.89.045001.

22. Pietras B, Daffertshofer A. Network dynamics of coupled oscillators and phase reduction techniques. Physics Reports. 2019;819:1–105. doi:10.1016/j.physrep.2019.06.001.

23. McFadden K, Steinmetz S, Carroll A, Simon S, Wallace A, Rojas D. EEG auditory steady state reliability paper. 2013;doi:10.6084/m9.figshare.829584.v14.

24. Rauschecker JP, Scott SK. Maps and streams in the auditory cortex: nonhuman primates illuminate human speech processing. Nature Neuroscience. 2009;12(6):718–724. doi:10.1038/nn.2331.

25. Reyes SA, Salvi RJ, Burkard RF, Coad ML, Wack DS, Galantowicz PJ, et al. PET imaging of the 40 Hz auditory steady state response. Hearing Research. 2004;194(1-2):73–80. doi:10.1016/j.heares.2004.04.001.

26. Ross B, Herdman AT, Pantev C. Right hemispheric laterality of human 40 Hz auditory steady-state responses. Cerebral Cortex. 2005;15(12):2029–2039. doi:10.1093/cercor/bhi078.

27. Ying J, Zhou D, Lin K, Gao X. Network analysis of functional brain connectivity driven by gamma-band auditory steady-state response in auditory hallucinations. Journal of Medical and Biological Engineering. 2015;35(1):45–51. doi:10.1007/s40846-015-0004-0.

28. Flandrin P, Goncalves P, Rilling G. Detrending and denoising with empirical mode decompositions. In: European Signal Processing Conference. vol. 06-10-Sept; 2004.

29. Flandrin P, Gonçalvès P, Rilling G. EMD equivalent filter banks, from interpretation to applications. vol. 5 of Interdisciplinary Mathematical Sciences. WORLD SCIENTIFIC; 2005. p. 57–74. Available from: `https://www.worldscientific.com/worldscibooks/10.1142/5862http://www.worldscientific.com/doi/abs/10.1142/9789812703347{_}0003`.

30. Molla MKI, Tanaka T, Rutkowski TM, Cichocki A. Separation of EOG artifacts from EEG signals using bivariate EMD. In: 2010 IEEE International Conference on Acoustics, Speech and Signal Processing. IEEE; 2010. p. 562–565. Available from: `http://ieeexplore.ieee.org/document/5495594/`.

31. Kayser J, Tenke CE, Gates NA, Kroppmann CJ, Gil RB, Bruder GE. ERP/CSD indices of impaired verbal working memory subprocesses in schizophrenia. Psychophysiology. 2006;43(3):237–252.

32. Gensler A, Sick B. Novel criteria to measure performance of time series segmentation techniques. CEUR Workshop Proceedings. 2014;1226(September 2014):193–204.

33. Kovács G, Sebestyen G, Hangan A. Evaluation metrics for anomaly detection algorithms in time-series. Acta Universitatis Sapientiae, Informatica. 2020;11(2):113–130. doi:10.2478/ausi-2019-0008.

34. Indola RP, Ebecken NFF. On extending F-measure and G-mean metrics to multi-class problems. WIT Transactions on Information and Communication Technologies. 2005;35:25–34.

35. O'Brien PC. Procedures for comparing samples with multiple endpoints. Biometrics. 1984; p. 1079–1087.

36. Cribben I, Haraldsdottir R, Atlas LY, Wager TD, Lindquist MA. Dynamic connectivity regression: determining state-related changes in brain connectivity. NeuroImage. 2012;61(4):907–920. doi:10.1016/j.neuroimage.2012.03.070.

37. Cribben I, Wager TD, Lindquist MA. Detecting functional connectivity change points for single-subject fMRI data. Frontiers in Computational Neuroscience. 2013;7(OCT). doi:10.3389/fncom.2013.00143.

38. Friedman J, Hastie T, Tibshirani R. Sparse inverse covariance estimation with the graphical lasso. Biostatistics. 2008;9(3):432–441. doi:10.1093/biostatistics/kxm045.

39. Sourty M, Thoraval L, Roquet D, Armspach JP, Foucher J, Blanc F. Identifying dynamic functional connectivity changes in dementia with lewy bodies based on product hidden Markov models. Frontiers in Computational Neuroscience. 2016;10(Jun):1–11. doi:10.3389/fncom.2016.00060.

40. Garnett R, Osborne MA, Reece S, Rogers A, Roberts SJ. Sequential bayesian prediction in the presence of changepoints and faults. Computer Journal. 2010;53(9):1430–1446. doi:10.1093/comjnl/bxq003.

41. Rasmussen CE, Williams CKI. Gaussian processes for machine learning. The MIT Press; 2005.

42. Heinonen M, Yildiz C, Mannerström H, Intosalmi J, Lähdesmäki H. Learning unknown ODE models with gaussian processes. 2018;.